13th International Symposium on Turbulence and Shear Flow Phenomena (TSFP13)
Montreal, Canada, June 25–28, 2024

EXPERIMENTAL STUDY ON THE MERGING OF TWO AXISYMMETRIC WAKES GENERATED BY POROUS DISCS

Ingrid Neunaber, R. Jason Hearst
Department of Energy and Process Engineering
Norwegian University of Science and Technology
Kolbjørn Hejes vei 2, 7034 Trondheim, Norway
ingrid.neunaber@ntnu.no, jason.hearst@ntnu.no

ABSTRACT

We investigated the wake merging and interaction downstream of two axisymmetric porous disks using hot-wire anemometry. Our study revealed that the strength of periodic vortex shedding signals in the spectra is enhanced when the wakes of different porous disks interact when compared to identical disks. This phenomenon warrants further detailed investigation due to its significance in understanding wake dynamics.

INTRODUCTION

The interaction of wakes poses a significant challenge, especially in scenarios like arrays of wind turbines or tidal turbines. It remains poorly understood, as highlighted in the review paper by van Kuik *et al.* (2016). Currently, wake interactions are often addressed using simplified superposition techniques, as demonstrated by Porté-Agel *et al.* (2020) and applied by inter alia Hegazy *et al.* (2022). One focus here is on the interaction of the wake of an upstream wind turbine with one or several downstream wind turbines and their wakes, e.g., (Torres Garcia *et al.*, 2019; Macrí *et al.*, 2021; Vad *et al.*, 2023). A second aspect is the interaction of wakes of closely spaced rotors for multi-rotor configurations (e.g., Maus *et al.* (2022) investigated the impact of spacing and the direction of rotation of two turbines by means of mean velocity, turbulent kinetic energy and the shape parameter).

In the field of turbulence, Obligado *et al.* (2022) recently illustrated how the axisymmetric wakes of two different types of discs, either fractal or square solid discs, with varying span-wise spacings interact. They identified three downstream regions in the interaction and turbulence evolution process, providing evidence of non-equilibrium turbulence, thus indicating complex turbulence interactions.

In the present study, we continue our exploration of the mixing of two axisymmetric wakes, using porous discs commonly employed as static substitutes for wind turbines, e.g., Neunaber *et al.* (2021). These porous discs reach a self-similar state earlier than solid discs (e.g., Lingkan & Buxton (2023) find self-similar behavior downstream of porous discs from $3D$ downstream, and Neunaber *et al.* (2022) show that the wake of a wind turbine in low-turbulent inflow exhibits self-similar behavior from $6.5D$ downstream). To examine turbulence interaction comprehensively, we investigate the effects of different span-wise spacings and disc types on wake mixing, and the data is investigated by means of mean velocity, turbulence intensity, power spectral density, and the shape factor.

EXPERIMENTAL SET-UP

The experiments were conducted in the low-speed wind tunnel at the Norwegian University of Science and Technology with dimensions of $1.8\,\mathrm{m} \times 2.7\,\mathrm{m}$ (height $\times$ width) and a test section length of 11 m. The inlet velocity was $U_i \approx 10\,\mathrm{ms}^{-1}$, and the free-stream turbulence intensity was $TI = u'/U < 0.3\%$ (with u' being the standard deviation of the velocity).

We present measurements taken downstream of a pair of porous discs with a diameter $D = 200\,\mathrm{mm}$, resulting in a diameter-based Reynolds number of approximately 125,000. In particular, we discuss the mixing of two wakes produced by identical discs with non-uniform blockage, referred to as disc type A, the mixing of two wakes generated by identical uniform mesh discs with uniform blockage, referred to as type B, and the mixing of two wakes generated by a set of different discs, consisting of one type A disc and one type B disc. Both discs have the same blockage, and their individual wakes were studied by (Vinnes *et al.*, 2022, 2023); the design of disc B was inspired by Camp & Cal (2016). It was shown that the wake of disc A expands and recovers significantly faster than the wake of disc B. Figure 1 provides photographs of both discs and their mounting; the discs were fixed to metallic rods with a diameter of 10 mm, which were secured at the top and bottom of the wind tunnel using tensioning screws to prevent vibrations.

For configuration AA (i.e., two discs of type A), we investigated three different spacings: $S = 1.5D$, $S = 2D$, and $S = 3D$, afterwards referred to as $AA-1.5$, $AA-2$ and $AA-3$. For configurations BB (i.e., two discs of type B) and AB (i.e., one disc of type A and one of type B), we examined $S = 2D$ (cf., Figure 1). Measurements were carried out using hot-wire anemometry. An automated traversing system moved the hot-wire through the wind tunnel, with the coordinate system indicated in Figure 1(a). Centerline measurements were conducted for $0.05 \leq x/D \leq 40$ downstream of the discs, with a spacing of $2D$ in the near field and $5D$ farther downstream. Additionally, span-wise profiles were measured at $x = 30D$ in the range of $-3.5 \leq y/D \leq 3.5$, with a spacing of $0.25D$ between points in the central part and $0.5D$ at the outer part. Furthermore, the reference velocity U_0 was measured at $y/D = 5$. Measurements were performed with a sampling frequency of $f_s = 75\,\mathrm{kHz}$ for $t = 180\,\mathrm{s}$, and a hardware low-pass filter was set at $f_{lp} = 30\,\mathrm{kHz}$. The hot-wire was calibrated before and after each span-wise profile or downstream measurement, and temperature correction according to Hultmark & Smits (2010) was applied.

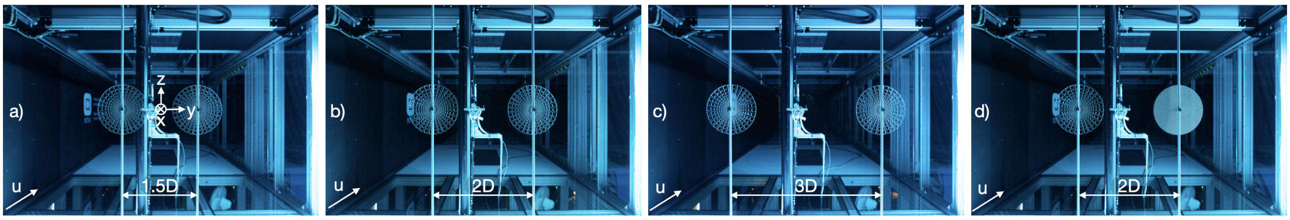

Figure 1. Photographs of the set-up looking downstream: (a) - (c) show the different spacings investigated for the configuration with two identical discs (type A), and (d) for two different discs (A and B). The hot-wire, mounted to a traverse, is centered between the discs. The coordinate system is indicated in (a).

RESULTS

In the following, first, the downstream centerline evolution of the mean velocity and the turbulence intensity will be discussed, followed by the span-wise mean velocity and turbulence intensity profiles at $x/D = 30$. For a better understanding of the turbulent structures, power spectral densities and the shape parameter λ^2 are discussed at $x/D = 30$.

Centerline Mean Velocity and Turbulence Intensity

Figures 2(a)-(c) present the downstream evolution of mean velocity, normalized by the mean velocity at the last measurement point, $U_0(x = 40D)$, for the AA cases, the BB case, and the AB case, respectively. Initially, for cases $AA-1.5$, $AA-2$, and AB, the mean velocity is about 15% higher than $U_0(x = 40D)$ but decreases rapidly, and drops below $U_0(x = 40D)$ before gradually converging towards it. From the evolution of the wake downstream of a single disc, cf. Vinnes *et al.* (2023), we can conclude that this behavior results from the wakes starting to interact near the discs ($5D - 10D$ downstream), where they are not fully evolved yet and the velocity deficits from both discs are still prominent. In contrast, both for the $AA-3$ case and for the BB case, the centerline mean velocity decreases consistently as the wakes evolve, recover, and eventually merge around $15D$ downstream.

In Figures 2(d)-(f), we show the downstream evolution of turbulence intensity at the centerline. Similar to the behavior observed downstream of single wakes generated by porous discs and wind turbines (e.g., Neunaber *et al.* (2021)), there is an initial increase in TI followed by a subsequent decrease. Based on the classification of wake regions detailed by Obligado *et al.* (2022), we can identify the region where the wakes are fully merged, indicated by decaying TI, from $x/D \approx 5, 10, 20$ for cases $AA-1.5$, $AA-2$, and $AA-3$, respectively. For the BB case, $x/D \approx 25$ and for the AB configuration, $x/D \approx 15$. This is consistent with the conclusions drawn from the evolution of the mean velocity evolution, and with the different wake recovery rates for the single wakes (Vinnes *et al.*, 2022, 2023). The maximum TI is influenced by the disc spacing; smaller spacings result in higher measured TI values. However, at $x/D = 40$, TI levels become similar across all cases, indicating that TI decays most rapidly for the smallest spacing. Notably, at the centerline, the AB configuration yields lower maximum turbulence intensities compared to the corresponding AA configuration, but higher turbulence intensities compared to the corresponding BB case. Overall, the evolution of TI is akin to what was observed by Obligado *et al.* (2022) for two sets of solid discs.

Span-wise Mean Velocity and Turbulence Intensity

In Figures 3(a)-(c), mean velocity profiles, normalized by freestream velocity U_0, are plotted at $x/D = 30$ for $-3.5 \leq y/D \leq 3.5$ for the AA cases, the BB case, and the AB case, respectively.
In the $AA-1.5$ and $AA-2$ configurations, the mean velocity profiles of the two discs merge into a single profile, resembling that of a single disc. Conversely, while the wakes have merged for the $AA-3$ case and for the BB case, the two peaks in velocity deficit originating from the individual wakes remain visible, with velocity minima at $y = \pm 1.5D$ and $y = \pm 1.0D$, respectively. In the AB configuration, wake asymmetry is evident due to differing recovery rates and expansion of the two discs, as discussed in Vinnes *et al.* (2023). From $y/D = -3.5$ to $y/D = -0.5$, downstream of disc A, the evolution mirrors that of the $AA-2$ configuration. However, a clear difference emerges as we move towards positive y, where velocity recovery downstream of the uniform disc B is slower. Notably, compared to the BB case, the velocity recovery downstream of the B-type disc is enhanced and the wake wider.

With respect to the turbulence intensity, as shown in Figure 3(d), for the AA configuration at $S = 1.5D$, the TI profile closely resembles the rather flat profiles of the single disc, cf. Vinnes *et al.* (2023), albeit with a more narrow central region. For $S = 2D$ and $S = 3D$, a relatively uniform distribution of TI is observed, decreasing at the wake boundaries but exhibiting a small region around $y/D \approx 0$ where the shear layers of the two wakes interact, resulting in slightly higher TI values. Again, this is consistent with findings in the single wake. In the BB case, Figure 3(e), the wakes of the two single discs are still identifiable, even with the shear layer peaks of the respective single discs. In the AB configuration, Figure 3(f), two distinct turbulence levels are identifiable downstream of the two discs, with turbulence downstream of disc B exceeding that of disc A, as shown by Vinnes *et al.* (2023), but lower than for the BB case. The highest turbulence intensities occur around $y/D \approx 0$, where the two wakes interact, as a consequence of an increase of u'.

Power Spectral Density

Figure 4 presents pre-multiplied Power Spectral Density (PSD) plots for various span-wise positions at $x/D = 30$ for all configurations. Notably, in Figures 4(a)-(c), the spectra for the central regions of the wakes in the AA configuration (all spacings), where TI profiles are relatively flat, collapse. In the outer wake regions, where TI is lower, the spectra naturally exhibit lower energy content. For the AA cases, at central wake positions, a peak is consistently observed at $f \approx 8.7$ Hz, indicating vortex shedding from the discs. The corresponding Strouhal number is $St = \frac{f \cdot D}{U_0} \approx 0.16$, similar to that of solid discs ($St \approx 0.135$) with an increase that has been observed

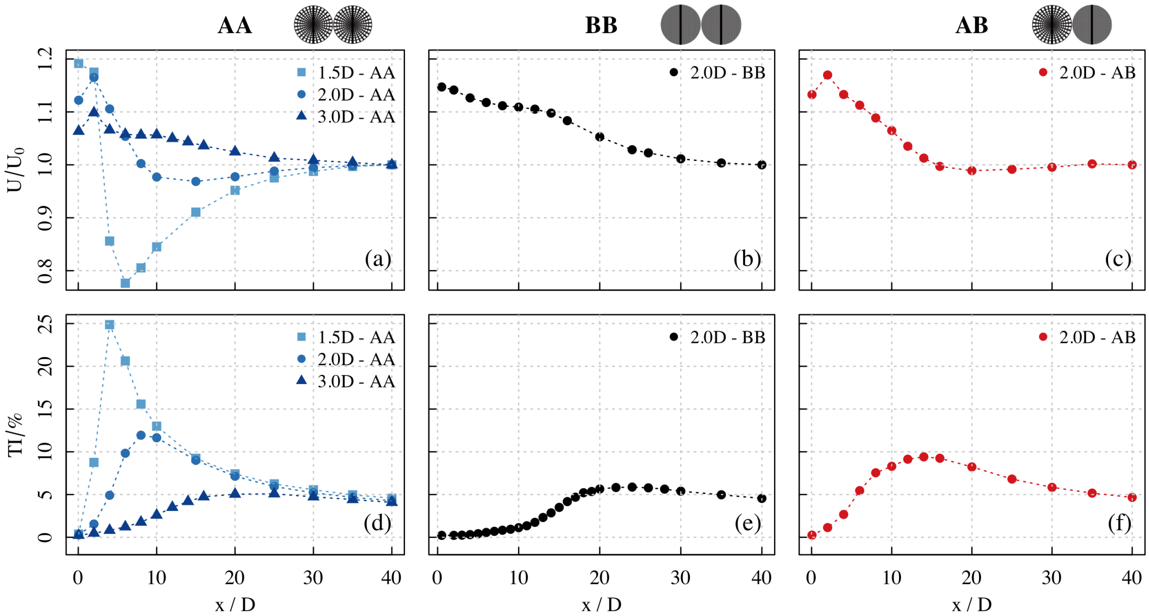

Figure 2. Evolution of the normalized mean velocity for (a) cases *AA*, (b) case *BB*, (c) case *AB*, respectively, and turbulence intensity for (d) cases *AA*, (e) case *BB*, (f) case *AB*, respectively, along the centerline.

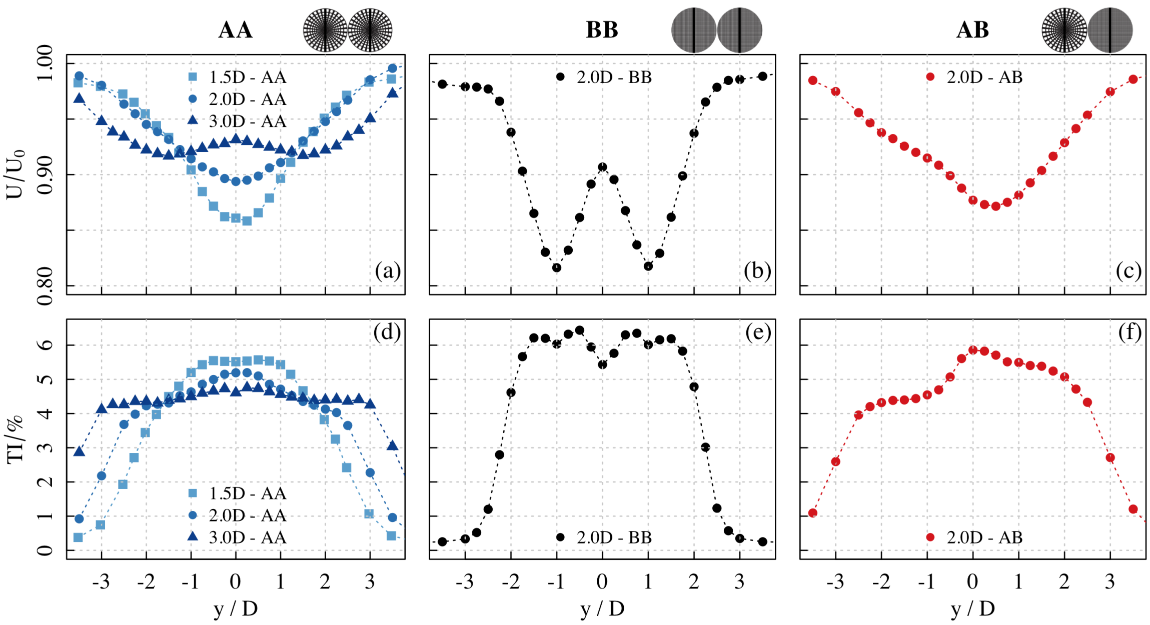

Figure 3. Normalized mean velocity profiles for (a) cases *AA*, (b) case *BB*, (c) case *AB*, respectively, and turbulence intensity profiles for (d) cases *AA*, (e) case *BB*, (f) case *AB*, respectively, at $x = 30D$.

for porous discs (Fuchs *et al.*, 1979; Theunissen & Worboys, 2018). The magnitude of this peak is relatively weak for all *AA* configurations, akin to the wake of a single type-*A* disc at $30D$, as shown in Vinnes *et al.* (2022). The spectra of the *BB* configuration, Figure 4(d), show significantly higher energy than all other cases for $y = \pm 0.5D$, which is consistent with the TI-levels at these positions. No vortex shedding peak is present, which is consistent with the results from Vinnes *et al.* (2022), who did not observe a vortex shedding peak for disc *B* at the centerline. In contrast, the *AB* configuration exhibits an enhanced vortex shedding peak at $y/D = 0$, $y/D = \pm 0.5$, and at $y/D = \pm 2$, and no peak observed downstream of the disc centers at $y/D = \pm 1$. This finding is particularly intriguing, as it expands the findings from Vinnes *et al.* (2022). These results suggest an alternative flow behavior where the periodicity between the disk wakes is enhanced and is thus worthy of further investigation. One possible explanation is that once the wake of disc *A* has expanded sufficiently, the oscillations are pushing and, thus, exciting the wake of disc *B*.

Shape Parameter

To add another dimension to the discussion of the interaction of wakes generated by porous discs, we investigate the evolution of the shape parameter $\lambda^2 = 1/4 \cdot \ln(\mathrm{F}(\delta u(t,\tau))/3)$, where F denotes the flatness, and $\delta u(t,\tau) = u(t+\tau) - u(t)$ the velocity increment with respect to the time scale τ (Castaing *et al.*, 1990; Chillá *et al.*, 1996). As a two-point statistical

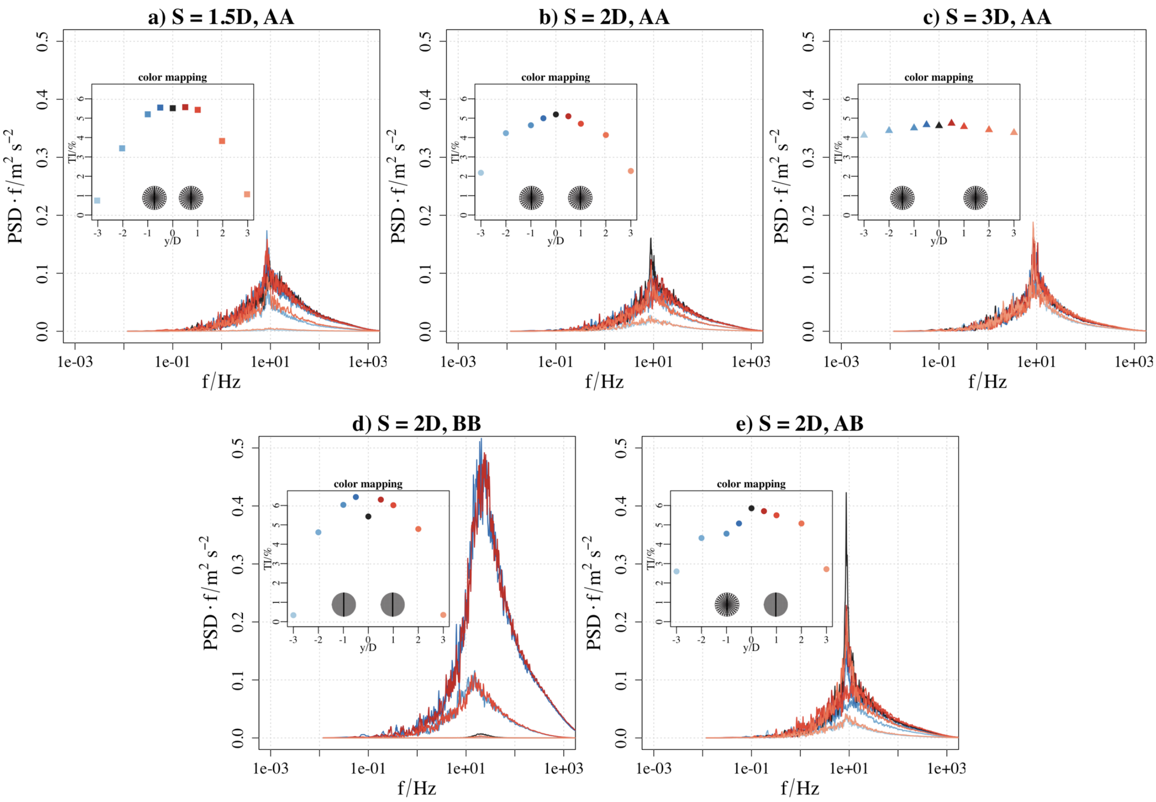

Figure 4. Pre-multiplied power spectral densities at different span-wise positions for the three spacings for case AA (a-c), the BB case (d), and the configuration with two different discs, case AB (e). The color scheme indicates span-wise positions and is given in the respective sub-plots of the span-wise TI at $x/D = 30$.

quantity, the shape parameter can be interpreted as a measure of the internal intermittency of a flow, and it can give insight into otherwise hidden flow features particularly at small time scales. If $\lambda^2 = 0$, the probability density function of the velocity increments is Gaussian and the flow is not intermittent, whereas the flow can be considered intermittent for $\lambda^2 > 0$. In that case, the probability density function of the velocity increments shows a higher probability for extreme fluctuations with respect to a certain time scale τ than predicted by a Gaussian distribution. For very large values, $\lambda^2 > 0.5$, the flow itself is not fully turbulent but intermittent. It has previously been shown that a ring of high intermittency is found both in the wake of a wind turbine and a single porous disc (Schottler *et al.*, 2018; Neunaber *et al.*, 2020; Vinnes *et al.*, 2023), as well as both in the outer part and the merging region of two wind turbines with lateral spacing (Maus *et al.*, 2022).

In Figures 5(a)-(e), the span-wise evolution of the shape parameter is plotted for multiple time scales τ, converted into spatial scales ρ by applying Taylor's hypothesis. For cases $AA-1.5$, $AA-2$, and AB, a central wake part can be observed for $-1 \leq y/D \leq 1$ where the shape parameter decreases from $\lambda^2(\rho/D = 0.01) \approx 0.2$ to $\lambda^2(\rho/D = 1) \approx 0$. This is typical of flows with features of homogeneous, isotropic turbulence and similar to results found in the central region of a single wake (Neunaber *et al.*, 2020; Vinnes *et al.*, 2023). Interestingly, the AB configuration shows a symmetrical pattern for λ^2 although both the velocity profile and the turbulence intensity profile are asymmetric (cf., Figure 3(c) and (f)). In the outer regions, λ^2 increases for all scales. A ring of high intermittency across all scales can be identified at the outer regions for these cases. For the $AA-3$ and BB cases, two individual wakes can be identified; while the spacing is too wide to clearly identify the intermittency ring in the $AA-3$ case, for the BB configuration, the onset of the intermittency ring is very sharp, in agreement with the narrower double-wake profile.

Overall, at $30D$, we find features of fully developed turbulence in the central region of the double wakes and the ring of high intermittency across all scales. In the central far wake wake region, intermittency is therefore only present for small scales, i.e., $\rho < D$.

CONCLUSION AND OUTLOOK

We have presented results from a hot-wire study of wake merging downstream of two types of porous discs in different combinations. We investigated the influence of span-wise spacing and disc type on the wake characteristics. Our findings indicate that maximum turbulence levels and the rate of turbulence decay are dependent on the disc spacing. Furthermore, combining two discs with different blockage distributions leads to an asymmetric wake with varying turbulence levels and an enhanced vortex shedding peak in the spectra. This suggests an alternative flow behavior compared to a set of identical discs where the wake of the non-shedding disc is excited by the wake of the shedding disc once they start interacting. To further advance the understanding of turbulence in the wake, we also investigate the internal intermittency of the wakes by means of the shape parameter, and in agreement with former studies, we identify a ring of high internal intermittency across all scales surrounding the double wake at $30D$ downstream. For all spacings and disc combinations, the turbulence in the central region exhibits classical behavior with a decreasing shape parameter, and vanishing intermittency for scales larger than the disc diameter.

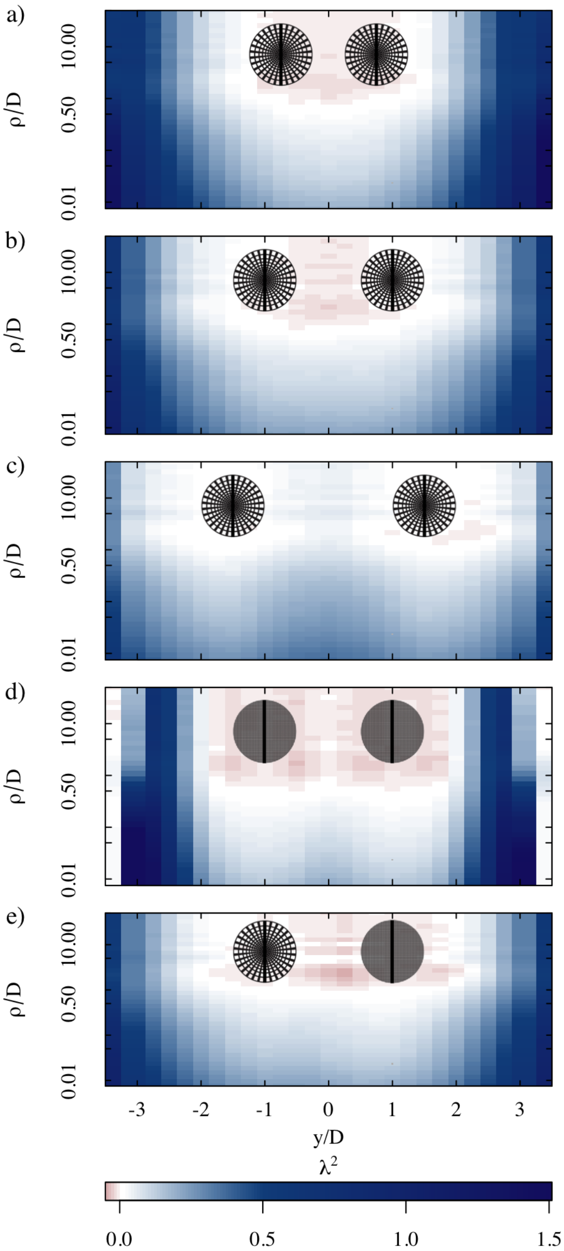

Figure 5. Span-wise evolution of the shape parameter $\lambda^2(\rho/D)$ at 30D downstream for (a) case *AA* and 1.5D spacing, (b) case *AA* and 2D spacing, (c) case *AA* and 3D spacing, (d) case *BB* and 2D spacing, and (E) case *AB* and 2D spacing.

REFERENCES

Camp, E. H. & Cal, R. B. 2016 Mean kinetic energy transport and event classification in a model wind turbine array versus an array of porous disks: Energy budget and octant analysis. *Physical Review Fluids* **1**, 044404.

Castaing, B., Gagne, Y. & Hopfinger, E. J. 1990 Velocity probability density functions of high reynolds number turbulence. *Physica D* **46** (177).

Chillá, F., Peinke, J. & Castaing, B. 1996 Multiplicative process in turbulent velocity statistics: A simplified analysis. *Journal de Physique II France* **6** (4), 455–460.

Fuchs, H. V., Mercker, E. & Michel, U. 1979 Large-scale coherent structures in the wake of axisymmetric bodies. *Journal of Fluid Mechanics* **93** (1), 185–207.

Hegazy, A., Blondel, F., Cathelain, M. & Aubrun, S. 2022 Lidar and scada data processing for interacting wind turbine wakes with comparison to analytical wake models. *Renewable Energy* **181**, 457–471.

Hultmark, M. & Smits, A. J. 2010 Temperature corrections for constant temperature and constant current hot-wire anemometers. *Measurement Science and Technology* **21**, 105404.

van Kuik, G. A. M., Peinke, J. & al. 2016 Long-term research challenges in wind energy a research agenda by the european academy of wind energy. *Wind Energy Science* **1** (1), 1–39.

Lingkan, E. H. & Buxton, O. R. H. 2023 An assessment of the scalings for the streamwise evolution of turbulent quantities in wakes produced by porous objects. *Renewable Energy* **209**, 1–9.

Macrí, S., Aubrun, S., Leroy, A. & Girard, N. 2021 Experimental investigation of wind turbine wake and load dynamics during yaw maneuvers. *Wind Energy Science* **6** (2), 585–599.

Maus, J., Peinke, J. & Hölling, M. 2022 Experimental investigation on the effect of lateral turbine spacing on interactions of wakes. *Journal of Physics: Conference Series* **2265**, 042064.

Neunaber, I., Hölling, M., Stevens, R. J. A. M., Schepers, G. & Peinke, J. 2020 Distinct turbulent regions in the wake of a wind turbine and their inflow-dependent locations: The creation of a wake map. *Energies* **13** (532).

Neunaber, I., Hölling, M., Whale, J. & Peinke, J. 2021 Comparison of the turbulence in the wakes of an actuator disc and a model wind turbine by higher order statistics: A wind tunnel study. *Renewable Energy* **179**, 1650–1662.

Neunaber, I., Peinke, J. & Obligado, M. 2022 Application of the Townsend–George theory for free shear flows to single and double wind turbine wakes – a wind tunnel study. *Wind Energy Science* **7** (1), 201–219.

Obligado, M., Klein, S. & Vassilicos, J. C. 2022 Interaction of two axisymmetric turbulent wakes. *Phys. Rev. Fluids* **7**, 114606.

Porté-Agel, F., Bastankhah, M. & Shamsoddin, S. 2020 Wind-turbine and wind-farm flows: A review. *Boundary-Layer Meteorology* **174** (1), 1–59.

Schottler, J., Bartl, J., Mühle, F., Sætran, L., Peinke, J. & Hölling, M. 2018 Wind tunnel experiments on wind turbine wakes in yaw: Redefining the wake width. *Wind Energy Science* **3**, 257–273.

Theunissen, Raf & Worboys, Robert 2018 Near-Wake Observations behind Azimuthally Perforated Disks With Varying Hole Layout and Porosity in Smooth Airstreams at High Reynolds Numbers. *Journal of Fluids Engineering* **141** (5), 051108.

Torres Garcia, E., Aubrun, S., Coupiac, O., Girard, N. & Boquet, M. 2019 Statistical characteristics of interacting wind turbine wakes from a 7-month lidar measurement campaign. *Renewable Energy* **130**, 1–11.

Vad, A., Tamaro, S. & Bottasso, C. L. 2023 A non-symmetric gaussian wake model for lateral wake-to-wake interactions. *Journal of Physics: Conference Series* **2505** (1), 012046.

Vinnes, M. K., Gambuzza, S., Ganapathisubramani, B. & Hearst, R. J. 2022 The far wake of porous disks and a model wind turbine: Similarities and differences assessed by hot-wire anemometry. *Journal of Renewable and Sustainable Energy* **14** (2), 023304.

Vinnes, M. K., Neunaber, I., Lykke, H-M H. & Hearst, R. J. 2023 Characterizing porous disk wakes in different turbulent inflow conditions with higher-order statistics. *Experiments in Fluids* **64** (2), 25.